Photon diffraction and interference

J.C. Hodge[1*]

[1]Blue Ridge Community College, 100 College Dr., Flat Rock, NC, 28731-1690

Abstract

Some observations of light are inconsistent with a wave–like model. Other observations of light are inconsistent with a traditional particle–like model. A single model of light has remained a mystery. Newton's speculations, Democritus's speculations, the Bohm interpretation of quantum mechanics, and the fractal philosophy are combined. The resulting model of photon structure and dynamics is tested by toy computer experiments. The simulations include photons from a distance, in Young's experiment, and from a laser. The patterns on the screens show diffraction patterns fit by the Fresnel equation. The model is consistent with the Afshar experiment.

Interference, Young's experiment, Afshar's experiment PACS 42.50Ct, 42.25Hz, 42.25.Fx

1 INTRODUCTION

A single model of light has remained a mystery. Black body radiation, the photoelectric effect, and the Compton effect observations reject the wave-in-space model of light. The reflection, diffraction, interference, polarization, and spectrographic observations reject the traditional particle model of light. The challenge of uniting the Newtonian and quantum worlds is to develop laws of motion of photons that obtain the diffraction experimental observations. The goal is to model a set of photon characteristics that can produce interference patterns.

The popular Copenhagen interpretation of quantum mechanics suggests the simultaneous existence of both apparently mutually exclusive concepts resulting in the principle of complementarity (wave–particle duality).

The Afshar experiment (Afshar 2005) may challenge the principle of complementarity in quantum mechanics. Coherent light was passed through dual pinholes, past a series of wires placed at interference minima, and through a condensing lens. The resulting images showed the dual pinholes that suggested the which-way information had been recovered.

---

*E-mail:jc_hodge@blueridge.edu

The Bohm interpretation of quantum mechanics is an alternative to the Copenhagen interpretation (Dürr,et al. 2009; Goldstein 2009). It is a causal, "hidden variable", and, perhaps, a deterministic model. Physics in the Newtonian and cosmological scales revolve around the concept that the motion of a single particle can be modeled. The Bohm interpretation posits particles have a definite position and momentum at all times. Particles are guided by a "pilot wave" in a Ψ–field that satisfies the Schrödinger equation, that acts on the particles to guide their path, that is ubiquitous, and that is non-local. The probabilistic nature of the Schrödinger equation results because measurements detect a statistical distribution. The origin of the Ψ–field and the dynamics of a single photon are unmodeled. The Ψ–field of Bohmian mechanics acts on particles and produces interference patterns with photons through slits.

Democritus of Abdera speculated that because different animals ate similar food, matter consists of an assembly of identical, smallest particles that recombine to form other types of matter. His term "atom" has been applied to an assembly of nucleons and electrons. Today, the Democritus concept applies as well to nucleons and smaller particles. Therefore, the Democritus "atom" is a still smaller, single type of particle.

That light moves slower through denser materials is well known. The index of refraction is the ratio of the speeds of light in differing media. Frizeau's experiment (Sartori 1996) measured a different speed of light between a medium moving toward a source and a medium moving away from a source. Both the "ether drag" model of Fresnel and the Special Theory of relativity are consistent with Frizeau's result. Because the index of refraction varies with the wavelength of light, refraction causes the analysis of light into its component wavelengths. This experimental observation is considered to decisively rule out the corpuscular model of light.

The gravitational lens phenomena may have two causes (Will 2001). The model for the gravitational lens phenomenon is that the convergent gravitational field (1) attracts light, (2) causes the curvature of coherent light, or (3) both. The gravitational attraction of photons was suggested in Newton's *Opticks* speculations. This produces a velocity $\vec{v}$ perpendicular to $\vec{c}$. This gravitational affect on light alone is insufficient to explain the gravitational lens phenomena yielding a calculated angular deviation approximately half the observed value.

The curvature-of-coherent-light model is that the light from stars is coherent and that coherence implies mutual attraction. An analogy is that of a rod with its axis maintained along the streamlines of the gravitational field. The rod travels perpendicular to its axis. The inner part of the rod slows or has a time dilation relative to the outer part. As light emerges from the convergent gravitational field, the rate of change in the direction of $\vec{c}$ and $\vec{v}$ decreases or is dampened. This is similar to the refraction of light by differing "media" densities. This model can account for the observed value of gravitational lensing (Eddington 1920, p. 209).

Models of photons have assumed the photon structure to be similar to other matter particles. That is, photons are assumed to be three-dimensional. The conclusion drawn from the well-known Michelson-Morley experiment's null re-

sult was that light is a wave, that there is no aether for light to "wave" in, and that a Fitzgerald or Lorentz type of contraction existed.

Fractal cosmology has been shown to fit astronomical data on the scale of galaxy clusters and larger (Baryshev and Teerikorpi 2002). At the opposite extreme, models such as Quantum Einstein Gravity have been presented that suggest a fractal structure on the near Planck scale (Lauscher and Reuter 2005). However, the Democritus' concept of the smallest particle suggests a lower limit of the fractal self-similarity.

The distinction between incoherent and coherent light is whether the light forms a diffraction/interference pattern when passed through one or more slits in a mask. Because interference has been thought to be a wave phenomenon, coherence is considered a property of waves. However, the definition of coherence allows a distribution of particles to be coherent.

Coherence is obtained (1) by light traveling a long distance such as from a star as seen in the Airy disk pattern in telescope images, (2) by the pinhole in the first mask in Young's experiment, and (3) from a laser.

Young's double-slit experiment has become a classic experiment because it demonstrates the central mysteries of the physics and of the philosophy of the very small. Incoherent light from a source such as a flame or incandescent light impinges on a mask and through a small pinhole or slit. The light through the first slit shows no diffraction effects. The light that passes through the slit is allowed to impinge on a second mask with two narrow, close slits. The light that passes through the two slits produces an interference pattern on a distant screen. The first slit makes the light coherent. The intensity pattern on the screen is described by the Huygens-Fresnel equation.

The assumptions of Fresnel model of diffraction include: (1) The Huygens' Principle that each point in a wave front emits a secondary wavelet. (2) The wavelets destructive and constructive interference produces the diffraction pattern. (3) The secondary waves are emitted in only the forward direction, which is the so called "obliquity factor" (a cosine function). (4) The wavelet phase advances by one-quarter period ahead of the wave that produced them. (5) The wave has a uniform amplitude and phase over the wave front in the slit and zero amplitude and no effect from behind the mask. (6) Note the Fresnel model has a slight arc of the wave front across the slit. That is, the distribution of energy in the plane of the slit varies. The Fresnel model with larger distance between the mask and the screen or with condensing lenses before and after the mask degenerates into the Fraunhofer diffraction model.

The intensity patterns produced by multiple slits can be compared to the intensities of the single slit pattern of equal total width. Thus, the resulting pattern may be regarded as due to the joint action of interference between the waves coming from corresponding points in the multiple slits and of diffraction from each slit. Diffraction in the Fresnel model is the result of interference of all the secondary wavelets radiating from the different elements of the wave front. The term diffraction is reserved for the consideration of the radiating elements that is usually stated as integration over the infinitesimal elements of the wave front. Interference is reserved for the superposition of existing waves, which is

usually stated as the superposition of a finite number of beams.

Sommerfield (1954) gave a more refined, vector treatment for phase application. However, these other more complex models make many simplifying assumptions. When the apertures are many wavelengths wide and the observations are made at appreciable distance from the screen, intensity results are identical to the Fresnel model.

Newton in his book Opticks (1730) speculated light was a stream (ray) of particles. The aether in query 17 overtakes (travels faster) the rays of light and directs the rays' path. Newton's analogy was of water waves. That is, Newton was using a self-similarity (fractal) postulate. The rays of light recede from denser parts of the aether in query 19. The aether grows denser from bodies in query 20 and this causes gravity in query 21. Newton seems to have suggested light is particles that are directed by the aether to produce the wave phenomena. The prevailing models of the 19th century considered light to be a wave. The prevailing interpretation of Newton's model is that Newton was suggesting light is both a wave and a particle rather than two entities having differing effects like a rock (photon) creating transverse waves in water (aether).

The Maxwell equations followed by the Special Theory of Relativity posited the velocity $\vec{c}$ of photons was constant in the absence of matter. This says nothing the speed of gravity (aether) waves.

The cosmological, scalar potential model (SPM) was derived from considerations of galaxies and galaxy clusters (Hodge 2004, 2006a,b,c,d,e) [1]. The SPM posits a plenum exists whose density distribution creates a scalar potential ρ (erg) field. The term "plenum" was chosen to distinguish the concept from "space" in the relativity sense and from "aether". The term "space" is reserved for a passive backdrop to measure distance, which is a mathematical construct. The plenum follows Descartes (1644) description of the plenum. The plenum is infinitely divisible, fills all volume between matter particles, is ubiquitous, flows to volumes according to the heat equation, is influenced by matter, is compressible in the sense that the amount of plenum in a volume may change, and influences matter.

Consideration of the electromagnetic signal of the Pioneer Anomaly led to the postulate that matter caused a depression in the plenum (Hodge 2006e). The redshift of the Pioneer Anomaly on the solar system scale ignored several terms because they had significant values only on the galactic scale (Hodge 2006e). In addition to the propositions of the galactic SPM, matter is posited to cause a static[2] warp in the ρ field in accordance with the Newtonian spherical property. "Static" because matter is neither a Source nor a Sink of energy. Because the ρ field near matter must attract other matter, the matter decreases the ρ field. The ρ field then causes matter attraction according to established gravitational physics and causes the frequency change of the EM signal[3]. Matter merely modifies the ρ energy flowing from Sources to Sinks. The SPM of the Pioneer

---

[1] A more complete discussion of this model is in Hodge (Theory of Everything)

[2] "Static" such as caused by a stationary electron in a stationary EM field.

[3] This concept is from General Relativity where matter shapes the geometrical "space" and "space" directs matter.

Anomaly is an effect on only the EM signal and is a blueshift superimposed on the Doppler redshift of the receding spacecraft.

Hodge (2004) showed that if the surface of the hod held $\rho = 0$, the ρ equipotential surfaces were ellipsoidal near the surface of the hod. The streamlines terminated on and perpendicular to the surface. Farther from the hod, the equipotential surfaces become spheres and the hod appears as a point at the center of the sphere. Newtonian equations apply at larger distance. The $\rho \geq 0$ always including the scale of photons and, possibly, atomic nuclei[4]. Because the hod has extent, the effect on ρ from a distance is treated as a negative ρ value at the center of the hod. Therefore, the $\rho < 0$ in matter equations reflects the hod having a surface area.

This Paper proposes a model of light that postulates the necessary characteristics of photons to satisfy observations and yield diffraction phenomenon. The model combines Newton's speculations, Democritus's speculations, the Bohm interpretation of quantum mechanics, and the fractal philosophy. The wave–like behavior of light results from the photons changing the Ψ–field that guides the path of the photons. The resulting model is tested by numerical simulation of diffraction and interference, with application to the Afshar experiment. Therefore, the wave characteristics of light may be obtained from the interaction of photons and Ψ–field.

In section 2, the model of photons is described and the equations are derived. Section 3 describes the computer simulation. Section 4 describes the computer simulation of photons traveling a long distance. Section 5 describes the computer simulation of Young's experiment. Section 6 describes the computer simulation of laser light. Section 7 describes the model application to the Afshar experiment. The Discussion and Conclusion are in section 8 and section 9, respectively.

2   Model

Newton's third law suggests that if the Ψ–field acts on photons, the photons and other matter should act on the Ψ–field.

Compare coherent light passing through multiple slits in a mask to light passing through a single slit. The slits may be viewed as transmitters of light that produces a diffraction pattern in the Ψ–field if the incoming light is coherent. The fractal philosophy of self-similarity suggests that the photons passing through a slit have similar elements that emit waves. If light is a particle, then the energy of a photon is smaller than the other known particles. Differing energy levels (color) among photons suggests light is an assembly of smaller, identical particles (hods). Like the Democritus's argument, the proportionality of mass and energy suggests mass is also an assembly of hods. Each photon must be coherent, must be emitting a diffraction pattern into the Ψ–field, and

---

[4]The action of the plenum on atomic nuclei at the largest was suggested by the differing Hα and HI galactic rotation curves (Hodge 2006c).

be composed of smaller emitters. That is, moving photons emit coherent forward waves in the Ψ–field like multiple slits. The analogy of a photon, of a slit, and of multiple slits is analogous to a linear antenna array of smaller emitters in a photon.

Photons exhibit gravitational effects caused by matter perpendicular to their direction of travel. The Michelson-Morley experiment suggests the hods and the photon have no resistance or drag in the Ψ–field in the direction of movement. This suggests the hod has zero thickness. Asymmetry in photon behavior near mass suggests asymmetry in photon structure. Therefore, the hod is a two dimensional object. The simplest structure that can produce a coherent wave is one hod next to another. Additional hods create a column of hods.

Each hod of a photon attracts Ψ at its surface to its maximum value. Between these hod surfaces and very near the hods of a photon, a $\Psi = 0$ surface is created. Beyond this surface, $\vec{\nabla}\Psi$ is directed first toward then away from a hod by the other hods. This holds the hods together. The Ψ–field cavitates as hods travel through the Ψ–field like an air foil traveling at the maximum speed through a gas.

If a hod transmits Ψ changes into the Ψ–field, the hod also receives changes in Ψ. The resulting force $\vec{F_s}$ of the Ψ–field acts on a hod to change $\vec{v}$ and to rotate the hod. The $\vec{v}$ is the result of a force $\vec{F_s}$ acting on the hod cross–section proportional to $\vec{n} \bullet \vec{\nabla}\Psi$ on the cross-section m_s of matter where $\vec{}$ indicates a vector in 3–space,

$$\vec{F_s} \propto m_s(\vec{n} \bullet \vec{\nabla}\Psi)\vec{n}, \tag{1}$$

where $\vec{n}$ is the surface, normal, unit vector. A vector without the $\vec{}$ indicates the value of the vector.

The Ψ change that results from the effect of other matter M on the Ψ–field is

$$\Psi = \sum_i^N GM_i/R_i, \tag{2}$$

where N is the number of bodies used in the calculation and R is the distance from the center of mass of M to the point where Ψ is measured. The R is large enough that the equipotential surfaces are approximately spherical. The M is linearly related to N_h where N_h is the number of hods in the body.

The gravitational lens phenomena suggest the photon's response to $\vec{\nabla}\Psi$ changes relative to the direction of $\vec{c}$. The Shapiro delay phenomena could be modeled as a decrease of c in a gravitational field. This also suggests c is a function of the gravitational field. The lower c suggested by the Shapiro delay in a lower Ψ–field causes a refraction in the direction of $\vec{c}$. The matter caused variation of the Ψ–field and the action of the Ψ–field on light causes $\vec{c}$ to change. The plane of the Michelson-Morley experiment was perpendicular to the Earth's surface and, therefore, in a nearly constant Ψ–field.

The $\vec{\nabla}\Psi$ produces the effect of gravity. The speed of the gravity wave (Ψ wave) that are changes in the force exerted by $\vec{\nabla}\Psi$ is much greater than c (van Flandern 1998). The development of Special Relativity was done using

electromagnetic experimental results. The speed limit of electromagnetic force changes is c. The higher speed of the $\vec{\nabla}\Psi$ wave is consistent with the quantum entanglement phenomena and is necessary if photons are to project the changing Ψ–field forward.

The redshift and blueshift of the Pound-Rebka experiment suggests a dependence of photon energy shift on the changing Ψ–field. That is, the energy of a photon is partly composed of the Ψ–field between the hods of the column as well as the number of hods in a photon. If the hods in a photon have no Ψ–field between them, the photon would have no third dimensional characteristics. Because a blueshift increase of energy occurs when Ψ decreases, because c decreases with Ψ, and if number N_{h} of hods in a photon remains constant, the inertial mass m_{I} of kinetic energy is posited to be

$$m_{\mathrm{I}} = N_{\mathrm{h}}(1 + K_{\Psi}\frac{\Psi_{\mathrm{max}}}{\Psi}), \tag{3}$$

where K_{Ψ} is a proportionality constant.

If c is much lower than the wave velocity of the Ψ–field, then the limiting factor of c may be like a terminal velocity. The Shapiro delay and the well known $E = mc^2$ relation combined with the lower Ψ near mass suggest for short range experiments,

$$c = K_{\mathrm{c}}(\frac{\Psi}{\Psi_{\mathrm{max}}})^2, \tag{4}$$

where K_{c} is the proportionality constant and Ψ_{max} is the maximum Ψ in the path of light wherein c is measured.

2.1 Hod action on Ψ–field

The action of all matter (hods) causes the Ψ to change. Therefore, the motion of a hod is relative to the local Ψ–field variation.

Matter causes the Ψ to decrease. Therefore the hod motion which pulls the Ψ to zero displaces the Ψ–field. The Ψ–field then flows back when the hod passes a point. That is, the hod's motion within a volume neither increases nor decreases the amount of Ψ–field in that volume. The cavitation in the Ψ–field produces a wave in the Ψ–field. The cavitation limits the c. The cavitation depends on the density of the Ψ–field, higher density allows a faster refresh of the Ψ round the hod and, therefore, a faster c than in a low Ψ–field. The wave has a $-\cos(kr)$ affect from the point of the hod center. Because the Ψ–field wave travels faster than the hod, the Ψ–field flows around the hod to fill in the depression behind the hod. If the speed of the wave in the Ψ–field is much larger than c, the harmonic wave is transmitted forward and the Ψ level behind the wave reaches a stable, non-oscillating level very rapidly and is the effect of gravity. This can be modeled as a $\cos(K_{\beta}\beta)$ decrease of Ψ's value, where β is the angle between the direction $\vec{c}$ of a hod and the direction of the point from the hod center where Ψ is calculated. The angle at which the Ψ–field no longer oscillates has the $\cos(K_{\beta}\beta) = 0$. This is analogous to the Fresnel model that

secondary wavelets are emitted in only the forward direction. Therefore, the effect on the Ψ–field of a single hod is

$$\Psi_{\text{single}} = \quad -\frac{K_r}{r} \cos\left(\frac{2\pi r}{\lambda_{\text{T}}}\right) \cos(K_\beta \beta) \exp^{-j(\omega t)} \quad K_\beta \beta < \pi/2$$

$$\Psi_{\text{single}} = \quad\quad\quad -K_r r^{-1} \quad\quad\quad\quad K_\beta \beta \geq \pi/2, \quad\quad (5)$$

where K_r is a proportionality constant, $j = \sqrt{(-1)}$, $\exp^{-j(\omega t)}$ is the wave time dependent component in the Ψ–field, and λ_{T} is the radial wavelength of the forward wave.

2.2 Ψ–field action on a hod

If energy may be transferred to the hods from the Ψ–field, then the motion of the hods may be dampened by the Ψ–field. Posit the dampening force is proportional to the Ψ, m_{s}, and $\vec{v}$ in analogy to non–turbulent movement through a medium. Non–turbulent flow is because the Ψ–field is ubiquitous and the speed of changes in the Ψ–field is much greater than c. Therefore,

$$m_{\text{I}} \dot{v} = K_{\text{v}} F_{\text{st}} - K_{\text{d}} m_{\text{s}} \Psi v, \quad\quad (6)$$

where the over dot means a time derivative, K_{v} and K_{d} are proportionality constants, $F_{\text{st}} \propto m_{\text{s}} |\vec{\nabla}\Psi| \sin(\theta)$, and θ is the angle between $\vec{\nabla}\Psi$ and $\vec{c}$.

Solving for v yields:

$$v_{\text{f}} = \frac{(A_{\text{vh}} + B_{\text{vh}} v_{\text{i}}) \exp^{B_{\text{vh}} \Delta t} - A_{\text{vh}}}{B_{\text{vh}}}, \quad\quad (7)$$

where t is the time of measurement, $v_{\text{i}} = v(\text{time} = t)$, $v_{\text{f}} = v(\text{time} = t + \Delta t)$, $A_{\text{vh}} = K_{\text{v}} m_{\text{s}} \vec{\nabla}\Psi \sin(\theta)/m_{\text{I}}$, and $B_{\text{vh}} = -K_{\text{d}} m_{\text{s}} \Psi/m_{\text{I}}$.

Posit the action of the Ψ–field on a single hod is acting with the same radial r component of the hod. The $\vec{r}$ is directed along the hod surface in the direction of $\vec{c}$. If the hod has a m_{s} and circular shape, $\dot{r} = 0$. The m_{s} and r are constant and the same for all hods. Because the hod is free to move, a change in orientation of the hod results in the hod changing direction. A differing $\vec{F}_{\text{s}}$ from one side of the hod surface to the other along $\vec{r}$ will cause a rotation of the hod. Assuming the hod is rigid is unnecessary, but convenient. If the $\vec{F}_{\text{s}}$ is close to $\vec{c}$, the rotation will be to align $\vec{c}$ with $\vec{F}_{\text{s}}$. If the $\vec{F}_{\text{s}}$ is close to the axis of the photon, the rotation will be to align the axis of the photon with $\vec{F}_{\text{s}}$. Define α as the critical angle between $\vec{c}$ and the angle at which $\vec{F}_{\text{s}}$ changes from acting to align with the axis to acting to align with $\vec{c}$. Because the dampening is in only the axial direction, the dampening caused by rotation is also proportional to the Ψ, m_{s}, and rotational velocity $\dot{\theta}$ in analogy to non–turbulent movement through a medium.

The torque from $\vec{F}_{\text{s}}$ is $rF_{\text{sa}} = K_{\theta \text{s}} m_{\text{s}} r |\vec{\nabla}\Psi| \sin(\theta)$ or

$$\frac{\text{d}}{\text{d}t}(r^2 m_{\text{I}} \dot{\theta}) = r F_{\text{sa}} - K_{\theta \text{d}} r m_{\text{s}} \Psi \dot{\theta}, \quad\quad (8)$$

Solving for $\dot{\theta}$ yields:

$$\dot{\theta}_{\mathrm{f}} = \frac{(A_{\theta\mathrm{h}} + B_{\theta\mathrm{h}}\dot{\theta}_{\mathrm{i}})\exp^{B_{\theta\mathrm{h}}\Delta t} - A_{\theta\mathrm{h}}}{B_{\theta\mathrm{h}}}, \tag{9}$$

where $\dot{\theta}_{\mathrm{i}} = \dot{\theta}(\text{time} = t)$, $\dot{\theta}_{\mathrm{f}} = \dot{\theta}(\text{time} = t + \Delta t)$,
$A_{\theta\mathrm{h}} = K_{\theta\mathrm{s}}m_{\mathrm{s}}|\vec{\nabla}\Psi|\sin(\theta)/rm_{\mathrm{I}}$,
$B_{\theta\mathrm{h}} = -K_{\theta\mathrm{d}}\frac{m_{\mathrm{s}}}{r}\frac{\Psi}{m_{\mathrm{I}}} - (\dot{m}_{\mathrm{I}}/m_{\mathrm{I}})$, and
$\dot{m}_{\mathrm{I}}/m_{\mathrm{I}}$ is small and nearly constant.

2.3 Photon action on Ψ–field

The suggested structure of the photon in Hodge (2004) implies each hod is positioned at a minimum Ψ because the hod surface holds the $\Psi = 0$. Therefore, the distance between hods in a photon is one wavelength λ_{T} of the emitted Ψ–field wave. Also, the hods of a photon emit in phase. Further, the number of hods in a photon and the Ψ–field potential Ψ_{max} due to all other causes around the hod effects this distance. Therefore, the transmitted potential Ψ_T from a photon is

$$\Psi_T = -\frac{K_r}{r}N_{\mathrm{effT}}, \tag{10}$$

where

$$N_{\mathrm{effT}} = \cos\left(\frac{2\pi r}{\lambda_{\mathrm{T}}}\right)\cos(K_\beta\beta)\left|\frac{\sin[N_{\mathrm{hT}}\pi\sin(\beta)]}{\sin[\pi\sin(\beta)]}\right| \quad K_\beta\beta < \pi/2$$
$$N_{\mathrm{effT}} = N_{\mathrm{hT}} \quad\quad\quad\quad\quad\quad\quad K_\beta\beta \geq \pi/2 \tag{11}$$

and $\lambda_{\mathrm{T}} = K_\lambda/(\Psi_{max}N_{\mathrm{hT}})$ and N_{hT} is the number of hods in the transmitting photon.

These equations apply to the plane that includes the center of the photon, the direction vector, and the axis of the photon.

2.4 Ψ–field action on a photon

The Ψ–field wave from each cause impinges on a photon through the hods. Because the photon is linearly extended, the photon is analogous to the receiving antenna. Therefore,

$$\vec{\nabla}\Psi_{\mathrm{eff}i} = \vec{\nabla}\Psi_i\left|\frac{\sin[\frac{N_{\mathrm{hR}}\pi\lambda_{\mathrm{T}i}}{\lambda_{\mathrm{R}}}\sin(\beta + \frac{2\pi\lambda_{\mathrm{T}i}}{\lambda_{\mathrm{R}}})]}{\sin[\pi\sin(\beta + \frac{2\pi\lambda_{\mathrm{T}i}}{\lambda_{\mathrm{R}}})]}\right|, \tag{12}$$

where N_{hR} is the number of hods in the receiving photon; λ_{R} is the wavelength, which is the distance between hods, of the receiving photon; and Ψ_i, $\lambda_{\mathrm{T}i}$, and $\vec{\nabla}\Psi_{\mathrm{eff}j}$ is the effective Ψ, λ_{T}, $\vec{\nabla}\Psi$, respectively, for the ith cause.

Using Eq. (12) in Eqns. (7) and (9) and summing the effect of all causes yields the total change in a Δt.

3   Simulation

A particle in the computer experiment was a set of numbers representing the points in position and momentum space whose motion was advanced in discrete time intervals of one calculation cycle. The particles position at the previous interval determines Ψ–field effect by the equations developed in section 2. The limitations of a computer experiment are caused by (1) noise from using a relatively small number of particles and the relative distances used, (2) bias caused by the approximate solution limitation of the number of digits, (3) the discrete time interval rather than continuous time progression, and (4) other possible effects. Understanding the results requires insight that can be obtained by experimental observation in the real world.

The simulation was conducted using a PC running a Visual Basic V program on the Windows XP platform. The horizontal axis (Y-axis) was the initial direction of the photons. The vertical axis (X-axis) was perpendicular to the initial photon direction. The nth photon p_{n} had X and Y position coordinates, $P_{\mathrm{x}}(p_{\mathrm{n}})$ and $P_{\mathrm{y}}(p_{\mathrm{n}})$, respectively, and the parameter values required by the equations. "Masks" were simulated by a range of y values at specified Y coordinates for all x values, a zone wherein photons were deleted, and a gap wherein photons were unchanged that defined the "slit". Each calculation was an "interval". Each "step" was one unit of distance measure along the X-axis or Y-axis. The values of $\Delta t = m_{\mathrm{s}} = 1$ were used. The $y = 0$ was the initial value of introduced photons. The $x = 0$ was the center of the initial photon distribution, the center of the one slit gap, and the center of the two slit gaps.

A "screen" was a virtual, vertical column positioned at a constant Y wherein the lower X coordinate x_{s} of the bin range determines the value that was recorded. Each X step was divided into 50 bins. As photons pass through the screen, the number $B(x_{\mathrm{s}})$ of photons at each bin was counted. Each photon was eliminated after being counted. Therefore, the accumulation of the number of photons through each bin over several intervals was the intensity of light at each bin. After 1000 photons were counted, x_{s} and $B(x_{\mathrm{s}})$ were recorded in an Excel file.

Because of the sampling error and of calculation errors noted above, the calculation of the best-fit Fresnel curve used an average

$$\bar{B}(x_{\mathrm{s}}) = \sum_{i=x_{\mathrm{s}}-0.1}^{i=x_{\mathrm{s}}+0.1} B(i)/11, \tag{13}$$

where i increments by 0.02 steps.

All the photons in these experiments were identical. That is, $N_{\mathrm{hT}} = N_{\mathrm{hR}} = 10$ and $\lambda_{\mathrm{T}} = \lambda_{\mathrm{R}}$. The constants in the equations are listed in Table 1 and were determined by trial and error. The difficulty in determining the constants was so the angle (x_{s}/L), where L (step) is the distance from the last mask to the screen, corresponded to the Fresnel equations. That is, so that $x = 1$ step and $y = 1$ step was the same distance of photon movement for the calculations, which is a Cartesian space.

Table 1: The values of the constants.

Parameter	value		units
K_{c}	1	$\times 10^{-8}$	step interval^{-1}
K_{Ψ}	1	$\times 10^{1}$	gr. hod^{-1}
K_{β}	1.1		
K_{r}	-8	$\times 10^{-11}$	erg step
K_{v}	1	$\times 10^{-5}$	
K_{d}	2.4	$\times 10^{-4}$	gr. step^{-2} erg^{-1} interval^{-1}
α	5	$\times 10^{-1}$	radian
$K_{\theta\mathrm{s}}$	6	$\times 10^{1}$	gr. interval^{-2} erg^{-1}
$K_{\theta\mathrm{d}}$	2	$\times 10^{1}$	gr. step^{-2} erg^{-1} interval^{-1}
K_{λ}	1	$\times 10^{-4}$	erg step hod
Ψ_{max}	1	$\times 10^{3}$	erg

Table 2 lists the curve fit measurements for the plots shown in the referenced figures. The first column is the figure number showing the curve. The second column is the number N_{c} of photons counted at the screen. The third column is the center of the theoretical curve (K_{cent}). The fourth column is the asymmetry A_{sym} of the data points (number of photons counted greater than K_{cent} minus number of photons counted less than K_{cent})/N_{c}. The fifth column is the sum of the least squares L_{sq} between the $\bar{B}(x_{\mathrm{s}})$ and the theoretical plot for -5 steps$\leq$ $x_{\mathrm{s}} \leq 5$ steps divided by N_{c}. The sixth column is the correlation coefficient between $\bar{B}(x_{\mathrm{s}})$ and the theoretical plot for -5 steps $\leq x_{\mathrm{s}} \leq 5$ steps.

4   Photons traveling a long distance

The initial distribution of photons was within a 60 steps by 60 steps section. One photon was randomly placed in each 1 step by 1 step part. The equations were applied to each of the photons in the section. Because the section has an outer edge, additional virtual photons were necessary to calculate the Ψ. Therefore, $[P_{\mathrm{x}}(p_{\mathrm{n}}),\ P_{\mathrm{y}}(p_{\mathrm{n}})]$, $[P_{\mathrm{x}}(p_{\mathrm{n}}),\ P_{\mathrm{y}}(p_{\mathrm{n}}) + 60]$, $[P_{\mathrm{x}}(p_{\mathrm{n}}),\ P_{\mathrm{y}}(p_{\mathrm{n}}) - 60]$, $[P_{\mathrm{x}}(p_{\mathrm{n}}) + 60,$ $P_{\mathrm{y}}(p_{\mathrm{n}})]$, $[P_{\mathrm{x}}(p_{\mathrm{n}})-60, P_{\mathrm{y}}(p_{\mathrm{n}})]$ $[P_{\mathrm{x}}(p_{\mathrm{n}})+60, P_{\mathrm{y}}(p_{\mathrm{n}})+60]$, $[P_{\mathrm{x}}(p_{\mathrm{n}})-60, P_{\mathrm{y}}(p_{\mathrm{n}})+60]$, $[P_{\mathrm{x}}(p_{\mathrm{n}})$-60, $P_{\mathrm{y}}(p_{\mathrm{n}}) - 60]$, and $[P_{\mathrm{x}}(p_{\mathrm{n}})+60, P_{\mathrm{y}}(p_{\mathrm{n}}) - 60]$ were included in the calculation of Ψ. Only photons and virtual photons within a radius of 30 steps were used in the calculation of Ψ at a point.

The equations were developed without consideration of photons colliding. That is, some photons were too close which generated very large, unrealistic Ψ values. Another characteristic of the toy model is that each interval moves a photon a discrete distance that occasionally places photons unrealistically close. When this happened, one of the close photons was eliminated from consideration. The initial distribution started with 3600 photons from which 111 were eliminated because of collision.

Figure 1(left) is a plot of the N_{effT} versus β with $N_{\mathrm{hT}} = 10$. The first five
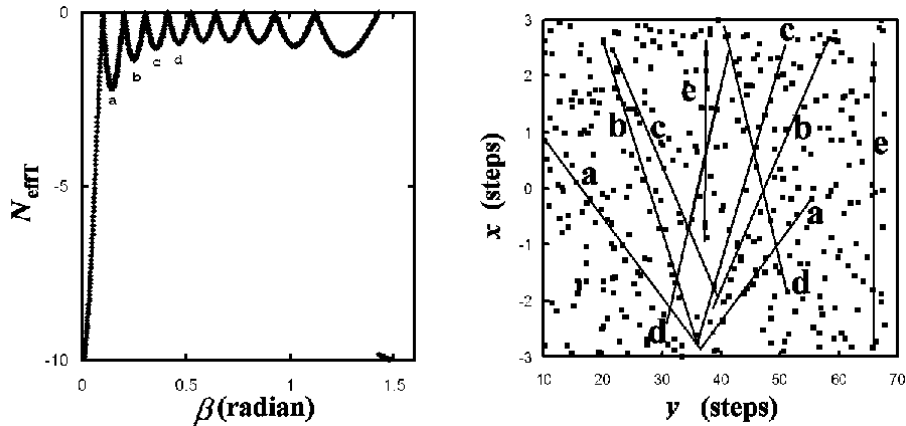
Figure 1: The left figure is a plot of the N_{effT} versus angle from the direction of the photon β $N_{\mathrm{hT}} = 10$. The first six minima are at $\beta = 0$ rad, 0.144 rad (a), 0.249 rad (b), 0.355 rad. (c), and 0.466 rad (d). The right figure is a plot of the longitudinal vs. latitudinal position of photons after 1000 intervals. The line labeled "e" is $\beta = \pi/2$. The lines are labeled as the angles in the left plot. The position of photons along lines corresponding to minima of a photons transmission pattern is what determines coherence.

peaks are at $\beta = 0$ rad, 0.144 rad (a), 0.249 rad (b), 0.355 rad. (c), 0.466 rad (d), and $\pi/2$ rad (e). This pattern is similar to the antenna emission pattern.

After 1000 intervals, a pattern of photon position developed as seen in Fig.1(right). The photons positions were recorded. The photons were organizing themselves into recognizable patterns of lines with angles to the direction of travel (Y axis) corresponding to the minima of Fig. 1(left).

A mask with a single slit with a width $W_{\mathrm{s}} = 1$ step was placed at $y = 100$ steps and a screen was placed at $y = 140$ steps ($L = 40$ steps). The positions of the photons were read from the recording. The group of photons were placed in 60 steps increments rearward from the mask. The photons were selected from the recording to form a beam width W_{in} (step) centered on the $x = 0$ step axis. Because the incoming beam had edges, the calculation for $P_{\mathrm{yold}}(p_{\mathrm{n}}) < 100$ was $P_{\mathrm{ynew}}(p_{\mathrm{n}}) = P_{\mathrm{yold}}(p_{\mathrm{n}}) + K_{\mathrm{c}} * 1$ interval, where $P_{\mathrm{yold}}(p_{\mathrm{n}})$ is the position of the nth photon from the last calculation and $P_{\mathrm{ynew}}(p_{\mathrm{n}})$ is the newly calculated position. The $P_{\mathrm{x}}(p_{\mathrm{n}})$ remained the same. If $P_{\mathrm{yold}}(p_{\mathrm{n}}) \geq 100$, the $P_{\mathrm{ynew}}(p_{\mathrm{n}})$ and $P_{\mathrm{x}}(p_{\mathrm{n}})$ were calculated according to the model.

Figure 2 shows the resulting patterns for varying W_{in}. The thicker, solid line in each figure is the result of a Fresnel equation fit to the data points. Although each plot shows a good fit to the Fresnel equation, the fit differs among the plots and depends on W_{in}. Because the calculation includes all photons, the photons that were destined to be removed by the mask have an affect on the diffraction pattern beyond the mask.
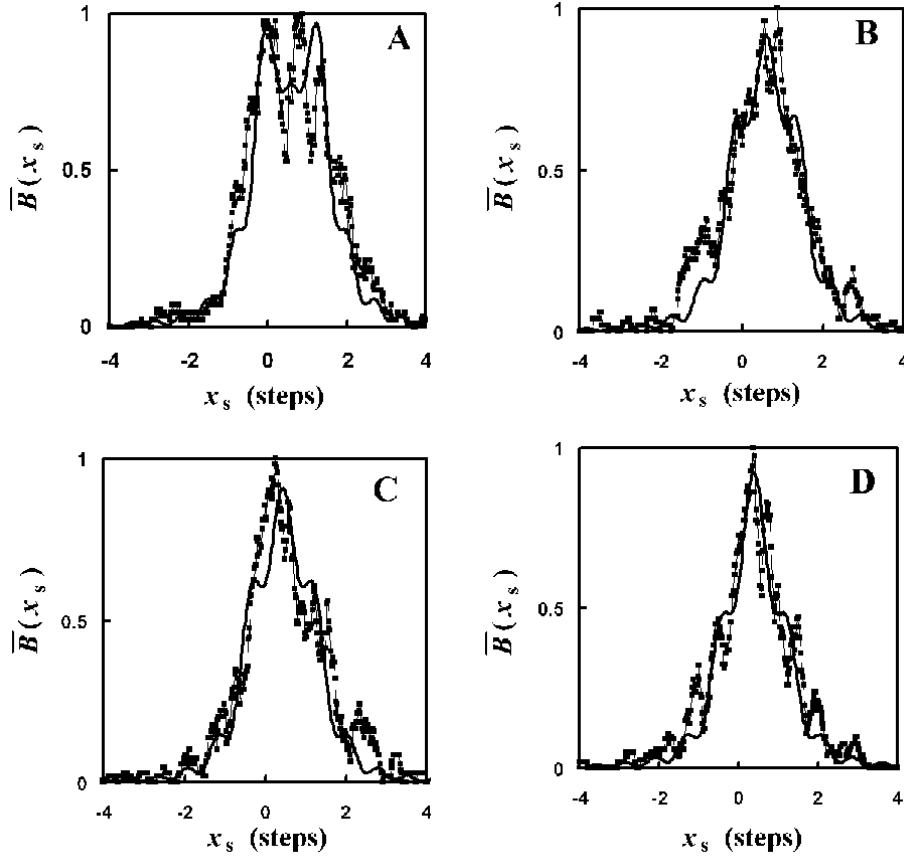
Figure 2: The single slit width $W_s = 1.0$ step screen patterns for $L = 40$ steps: (A) input beam width $W_{in} = 1.0$ step which is the same as the slit width, (B) $W_{in} = 2.0$ steps, (C) $W_{in} = 4.0$ steps, and (D) $W_{in} = 6.0$ steps. The filled squares are the data points, the thin line connects the data points, and the thick line marks the theoretical calculation. Although each plot shows a good fit to the Fresnel equation, the fit differs among the plots and depends on W_{in}. Because the calculation includes all photons, the photons that were destined to be removed by the mask have an effect on the diffraction pattern beyond the mask.

Table 2: The measurements of the curve fit.

Fig.	N_c [a]	K_{cent} [b]	A_{sym} [c]	L_{sq} [d]	C_c [e]
2A	1000	0.585	0.014	0.219	0.96
2B	1000	0.605	-0.028	0.199	0.97
2C	1000	0.408	0.000	0.247	0.96
2D	1000	0.383	0.006	0.259	0.96
3A	1000	0.259	0.084	0.360	0.97
3B	1000	0.426	0.050	0.021	0.92
3C[f]	1000	0.271	0.060	0.185	0.98
3D[f]	1000	0.535	0.006	0.246	0.83
5A	438	0.187	-0.046	0.178	0.92
5B	1000	0.314	-0.070	0.717	0.82
8	400	0.850	-0.320	0.221	0.68
9	1000	0.145	-0.122	0.909	0.79
11	1000	0.273	-0.074	0.895	0.81

[a] The number of photons counted at the sceen.
[b] The center of the theoretical curve.
[c] The (number of photons counted greater than K_{cent} minus number of photons counted less than K_{cent})/N_c.
[d] The sum of the least squares between the $\bar{B}(x_s)$ and the theoretical plot for -5 steps $\leq x_s \leq$ 5 steps.
[e] The correlation coefficient between $\bar{B}(x_s)$ and the theoretical plot for -5 steps $\leq x_s \leq$ 5 steps.
[f] This curve is relative to a Fraunhofer equation fit.

Figure 3 shows the resulting patterns for varying L. The mask, screen, and photon input was the same as the previous experiment with $W_{\text{in}} = 6$ steps. Comparing Fig. 3(A), Fig. 2(D), and Fig. 3(B) shows the evolution of the diffraction pattern with $L = 30$ steps, $L = 40$ steps, and $L = 50$ steps, respectively. Fig. 3(C) and Fig. 3(D) show the Fraunhofer equation fits. The greater L produces a closer match between the Fresnel and Fraunhofer equation fits.

Figure 4 shows an expanded view of Fig. 3(B). The center area, first ring, and second ring of Fig. 3(B) and Fig. 4 has 954 photons, 20 photons, and 4 photons, respectively, of the 1000 photons counted.

Figure 5 shows the screen pattern with the mask from the previous experiment replaced by a double slit mask. Figure 5(A) was with the slits placed from 0.50 step to 1.00 step and from -1.00 step to -0.50 step. The best two slit Fresnel fit (a cosine term multiplied be the one slit Fresnel equation) is expected for slits with a ratio of the width b of one slit to the width d between the centers of the slits (the "d/b ratio"). Figure 5(B) shows the screen pattern with the slits placed from 0.75 step to 1.25 steps and from -1.25 steps to -0.75 step.

Figure 6 shows the paths traced by 10 consecutive photons through the slits at two different intervals that form part of the distribution of Fig. 5A. The traces are from the mask to the screen. The θ for each photon is established after $y = 130$ steps. Before $y = 120$, there is considerable change in θ, which is consistent with Fig. 3. That is, the photon paths do not start at the slit and follow straight lines to the screen. The Fresnel equation applies only after some distance from the mask.

The numbers in Fig. 6 mark the following occurrences: (1) One photon follows another and traces the same path. The following photon travels a longer path before path merging. (2) One photon follows another and traces a parallel and close path. (3) A photon experiences an abrupt change in θ as it passes close to another photon. These events were probably a result of the discrete nature of the simulation like the collision condition noted previously. (4) A photon from one slit follows another from the other slit. The leading photon determines the x_{s} and θ at the screen.

5   Young's experiment

The input to Young's experiment was at 0 step $\leq y \leq 1$ step and -3 steps $\leq x \leq$ 3 steps. A photon is placed at random in each 1 step X 1 step area. The input was repeated every 100 intervals. The first mask was place at $y=100$ steps with $W_{\text{s}} = 1$ step centered on the X-axis. If a photon's $P_{\text{y}}(p_{\text{n}}) \leq 100$ step, then $P_{\text{ynew}}(p_{\text{n}}) = P_{\text{yold}}(p_{\text{n}}) + K_{\text{c}} * 1$ interval. If a photon's $P_{\text{yold}}(p_{\text{n}}) > 100$ step, then the new position was calculated in accordance with the model.

A screen placed at $y= 140$ steps showed a rounded pattern between -4 steps $\leq x_{\text{s}} \leq 4$ steps. Comparison with Fig. 2 diffraction patterns shows Fig. 7 is not a diffraction pattern for $L = 40$ steps.

Figure 7 (right) shows the distribution of photons between the first mask and the screen. The lines and the lower case letters are as in Fig. 1.
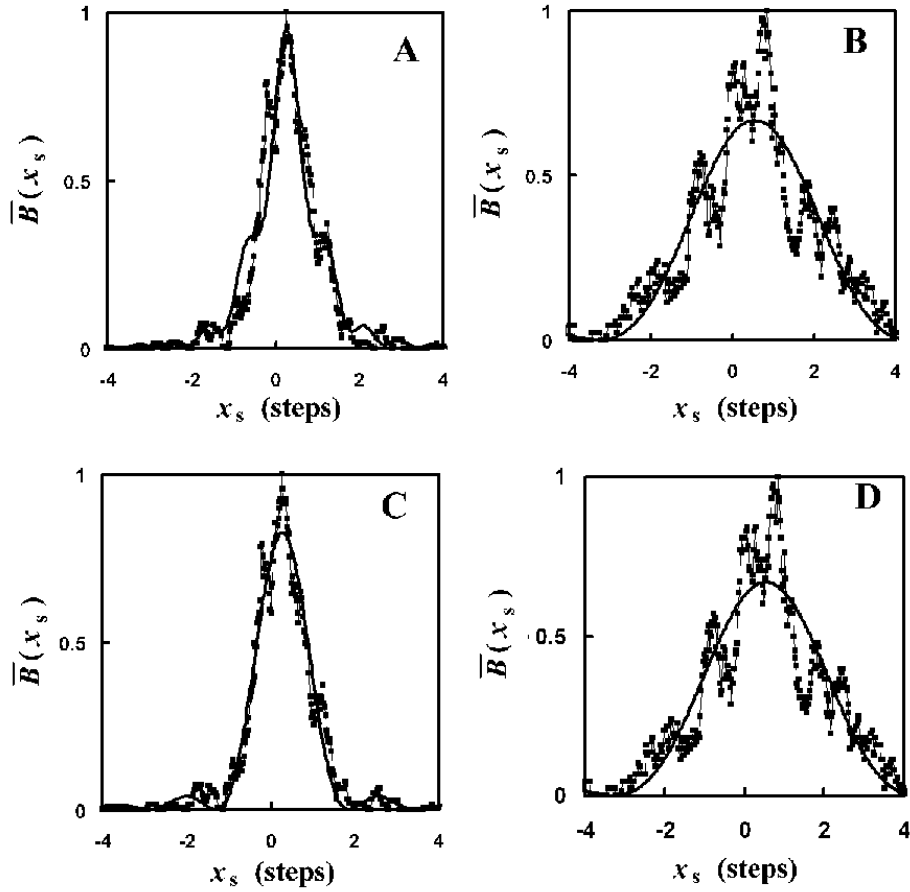
Figure 3: Resulting patterns for varying L. The mask, screen, and photon input was the same as the previous experiment with $W_{in} = 6$ steps. The single slit $W_s = 1.0$ step screen patterns for $L = 30$ steps (left figures A and C) and for $L = 50$ steps (right figures B and D). The top row is the Fresnel calculation plots and the bottom row is the Fraunhofer calculation plots. The filled squares are the data points, the thin line connects the data points, and the thick line marks the theoretical calculation. Comparing Fig. 3(A), Fig. 2(D), and Fig. 3(B) shows the evolution of the diffraction pattern with $L = 30$ steps, $L = 40$ steps, and $L = 50$ steps, respectively. Fig. 3(C) and Fig. 3(D) show the Fraunhofer equation fits. The greater L produces a closer match between the Fresnel and Fraunhofer equation fits.
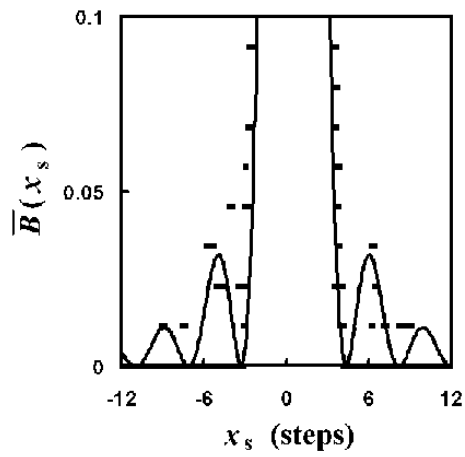
Figure 4: Plot of Fig. 3B with an expanded scale to show the second and third diffraction rings. The filled squares are the data points, the thin line connects the data points, and the thick line marks the theoretical calculation. The center area, first ring, and second ring of Fig. 3(B) and Fig. 4 has 954 photons, 20 photons, and 4 photons, respectively, of the 1000 photons counted. The number of photons in each ring agrees with the theoretical calculation of the relative intensity of the diffraction rings.
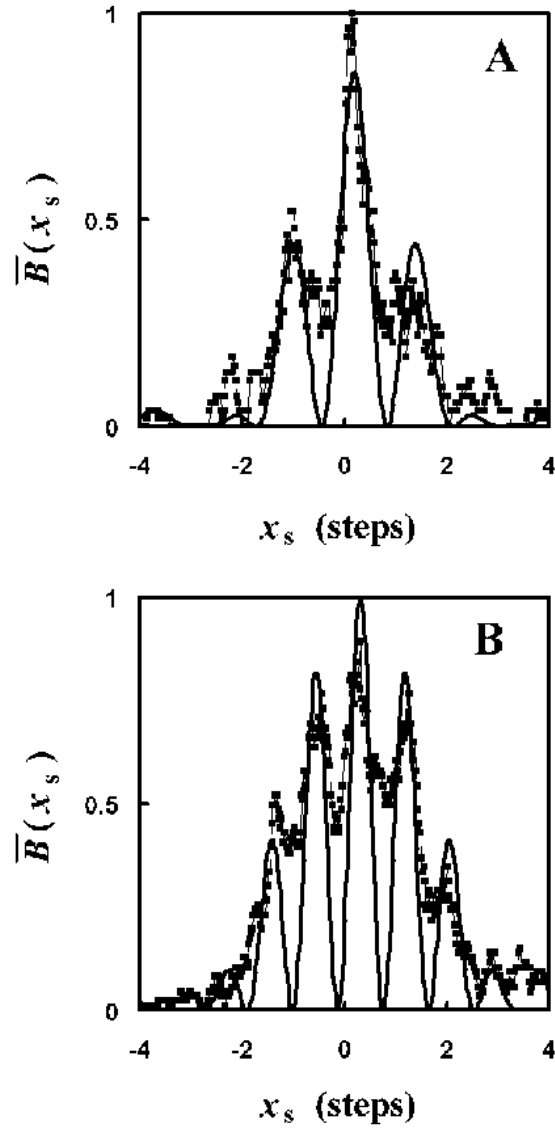
Figure 5: Plot of the double slit screen pattern at $L = 40$ steps and $W_{in} = 8$ steps. The A figure is with the slits placed from 0.50 step to 1.00 step and from -1.00 step to -0.50 step. The B figure is with the slits placed from 0.75 step to 1.25 steps and from -1.25 steps to -0.75 step. The filled squares are the data points, the thin line connects the data points, and the thick line marks the theoretical calculation. The model produces the double slit interference pattern.
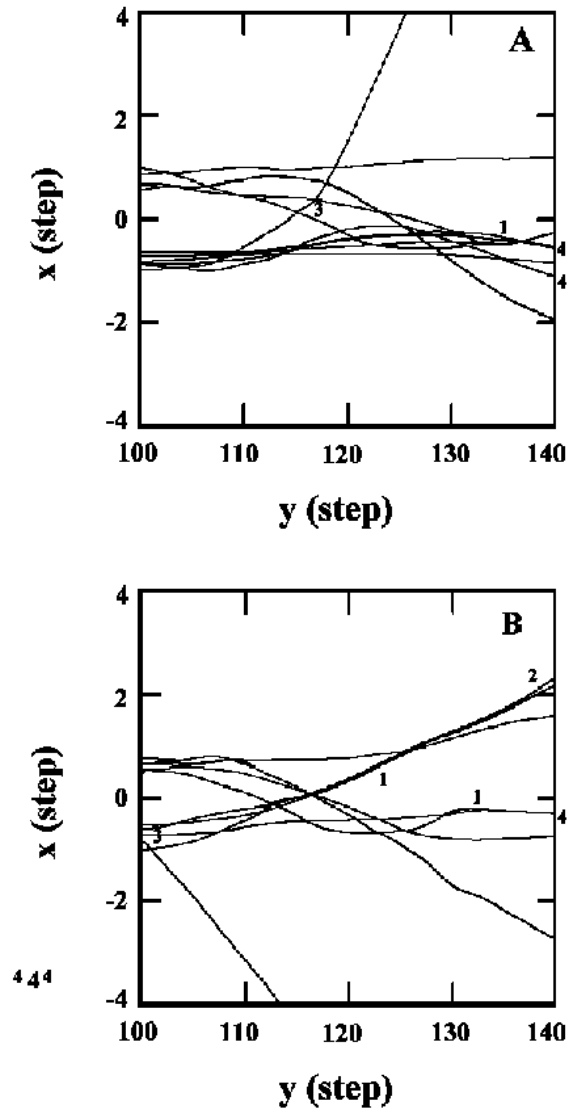
Figure 6: Traces of 10 consecutive photon paths between the mask and screen at two different intervals. The numbers mark the following occurrences: (1) One photon follows another and traces the same path. The following photon travels a longer path before path merging. (2) One photon follows another and traces a parallel and close path. (3) A photon experiences an abrupt change in θ as it passes close to another photon. These events were probably a result of the discrete nature of the simulation like a collision condition. (4) A photon from one slit follows another from the other slit. The leading photon determines the x_s and θ at the screen. The photon's path continues to change direction for a short distance after the mask.
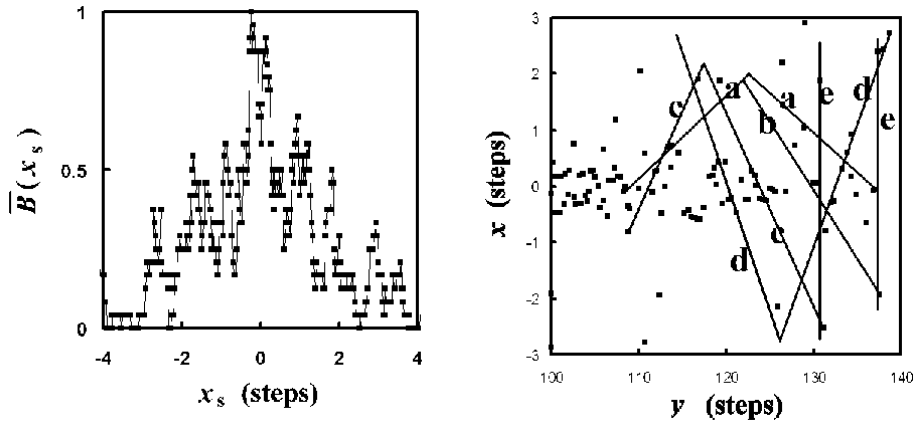
Figure 7: The right figure is a plot screen pattern of Young's experiment at $L = 40$ steps after the first mask and $W_{\text{in}} = 6$ steps. The filled squares are the data points. The thin line connects the data points. The Fresnel equation fit is poor. Therefore, the pattern is not a diffraction pattern. The right figure shows the distribution of photons from the first mask to the screen. The lines and the lower case letters are as in Fig. 1. Random photons through a first slit fail to produce a diffraction pattern that indicates incoherence. However, the position distribution shows coherence (see Fig. 1B).

The screen was removed and the second mask was placed at $y = 140$ steps. The second mask had two slits placed 0.5 step $\leq x \leq$ 1.0 step and at -1.0 step $\leq x \leq$ -0.5 step. The screen was placed at $y = 180$ steps ($L = 40$ steps). Figure 8 shows the resulting distribution pattern.

Although the statistics for Fig. 8 are poorer than previous screen interference patterns, inspection of Fig. 8 indicates an interference pattern was obtained. Figure 3(B and D) after 50 steps of calculation compared with Figure 3(A and C) after 30 steps of calculation indicates that the calculation errors are causing increased and noticeable scatter after 50 steps of calculation. Figure 8 is after 80 steps of calculation.

6   Laser

The initial, overall photon density in the previous sections was approximately uniform and incoherent. The photons in the distance simulation or the slit in the Young's simulation formed the coherent distribution. These coherent distributions resulted from an application of the model to an initial random distribution.

The popular model of a laser is that a seed photon in a medium stimulates the emission of more photons. Because the photons from a laser impinging
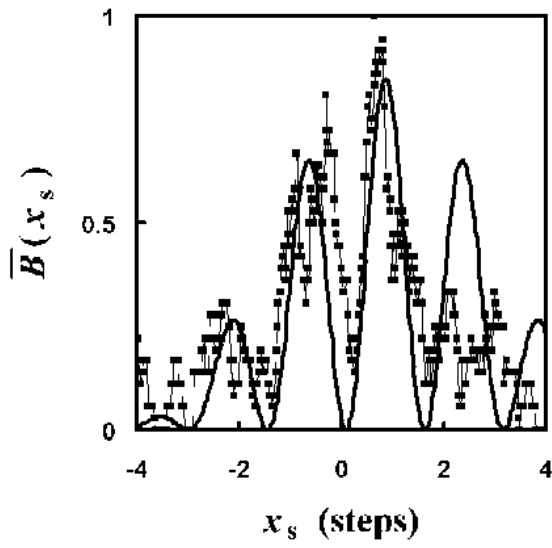
Figure 8: Plot of the double slit screen pattern at $L = 40$ steps from the second mask and 80 steps beyond the first mask. The slits were placed from 0.50 step to 1.00 step and from -1.00 step to -0.50 step. The filled squares are the data points, the thin line connects the data points, and the thick line marks the theoretical calculation. The position distribution after the first mask is coherent.
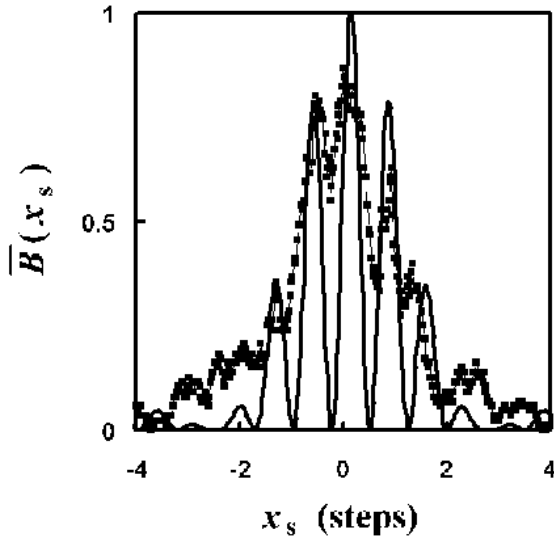
Figure 9: Plot of the pattern on a screen at $L = 40$ steps of a laser pulse input $W_{in} = 6$ steps through a double slit. The slits were placed from 0.50 step to 1.00 step and from -1.00 step to -0.50 step. The filled squares are the data points, the thin line connects the data points, and the thick line marks the theoretical calculation.

on a slit(s) produces a diffraction pattern, the laser simulation must produce the coherent distribution of photons. Because of the diversity of materials that produce laser emissions, the laser must form an ordered distribution within the light.

The Fourier transform of a triangular function is the sinc-type function. Another function with a Fourier transform of the sinc-type function is the rectangular function. If the slit acts as a Fourier transform on the stream of photons, a pulse pattern with high density and a low duty cycle may also produce the diffraction pattern.

A simple model of the simulation of the laser light is several photons followed by a delay between pulses. Figure 9 shows the result of passing a pulse through a double slit. The pulse is formed by positioning a photon randomly in half step x intervals and randomly within a 1.1 steps y interval. These pulses were three steps apart and $W_{in} = 6$ steps. Several other pulse configurations were tried and yielded a poorer fit. The parameters are unique. Also, the fit is inconsistent with observation of interference patterns for a d/b ratio of 3/1. That this is what lasers in general produce seems unlikely.

That the photons form lines with a set angle to $\vec{c}$ was noted in Fig. 1 and Fig. 7. Posit that a seed photon follows a free photon in the laser material. These photons form themselves at an angle noted in Fig. 1. The angles are
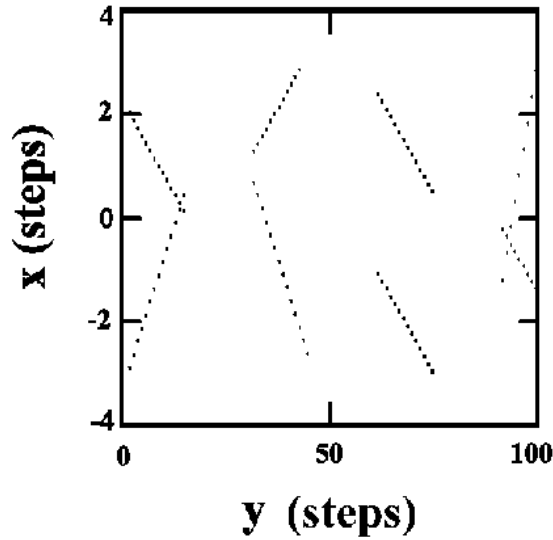
Figure 10: Plot of the position of photons between 0 step$\leq y \leq$ 100 steps and $W_{\text{in}} = 6$ steps.

related to N_{h}. These photon then exert a force along the angle to free weakly bound photons. Thus, a line of photons is formed. The lines are then emitted.

The experiment was to create two seed photons at $y = 0$ and randomly between -3 steps $\leq x \leq$ 3 steps. A line of 13 additional photons was introduced from each of the seed photons at one of the four angles, which was randomly chosen, progressing positively or negatively. Figure 10 depicts a plot of such a distribution at one interval. This model has the advantage of being dependent on N_{h} and the form of the distribution produced by distant travel and by the first slit in Young's experiment.

The photons were then directed to a mask at $y = 100$ with a double slit. The slits placed from 0.50 step to 1.00 step and from -1.00 step to -0.50 step.

The fit is consistent with observation of interference patterns for a d/b ratio of 3/1.

7   Afshar experiment

The Afshar experiment involves a wire grid and lenses in addition to a screen. Placing thin wires of one bin thickness at minima is possible in the present experiment. The $\bar{B}(x_{\text{s}})$ values averaged 11 bins. There were bins with no photons near the minima.

The modeling of the photon interacting with matter and lenses is for a future paper. Therefore, the x_{s} and the angle ϕ_{s} of $\vec{c}$ to the Y axis was also recorded
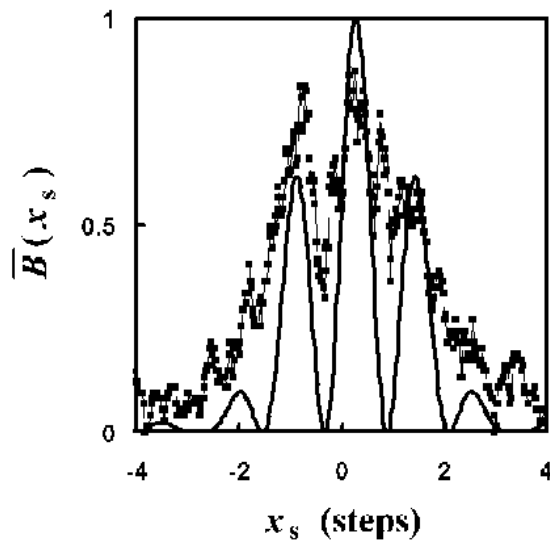
Figure 11: Plot of the pattern on a screen at $L = 40$ steps of a line laser input (see Fig. 10) $W_{\mathrm{in}} = 6$ steps through a double slit. The slits placed from 0.50 step to 1.00 step and from -1.00 step to -0.50 step. The filled squares are the data points, the thin line connects the data points, and the thick line marks the theoretical calculation.
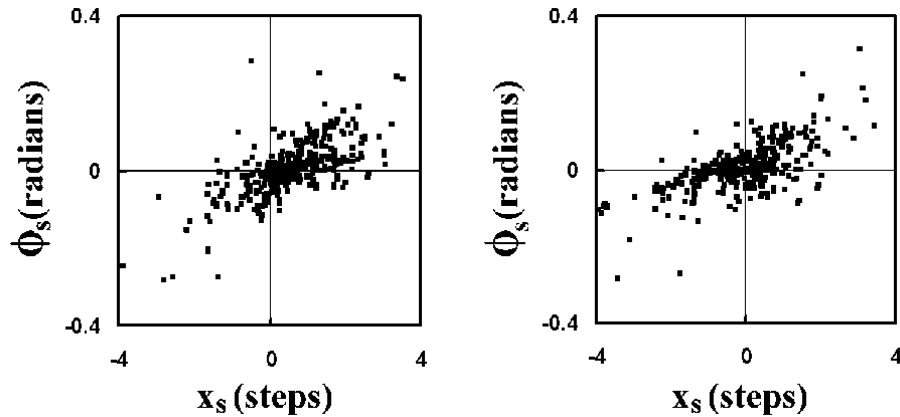
Figure 12: Plot of ϕ_s vs. x_s for the photons that passed through the Positive Slit (left) and the photons that passed through the Negative Slit (right). The groups of photons with -3 steps $\leq x_s \leq 3$ steps to have a nearly linear distribution. A linear regression was done on the data of each of the groups. Photons existed outside this range. However, occurrences (1) and (2) of Fig. 6, which was considered an artifact of the simulation, caused errors. The distribution outside this range became non-linear. Over 86% of the recorded photons were in this range.

when a photon was counted at the screen.

Figure 12 shows a plot of ϕ_s vs. x_s for the photons that passed through the slit at 0.5 steps $\leq x_s \leq 1.0$ steps (the "Positive Slit") and the photons that passed through the slit at -1.0 steps $\leq x_s \leq$ -0.5 steps (the "Negative Slit").

Figure 12 shows the groups of photons with -3 steps $\leq x_s \leq 3$ steps to have a nearly linear distribution. A linear regression was done on the data of each of the groups. Photons existed outside this range. However, occurrences (1) and (2) of Fig. 6, which was considered an artifact of the simulation, caused errors. The distribution outside this range became non-linear. Over 86% of the recorded photons were in this range.

$$\phi_s = mx_s + b, \tag{14}$$

where m is the slope and b is the intercept of the linear regression.

Table 3 lists the resulting values of the linear regression equation for each of the data sets and the calculated ϕ_s at $x_s = 2$ steps and $x_s = 2$ steps. The majority of the photons impinge on the screen at angles that would cause a condensing lens to focus them at different points associated with the slits. Figure 6, occurrence (4) showed some photons from one slit follow another photon from the other slit and, therefore, were recorded with the ϕ_s as if from the wrong slit. This occurred for both slits. Therefore, the statistical effect would balance.

The majority of the photons impinge on the screen at angles that would

Table 3: The values of the constants in the linear regression Eq. 14.

slit	m rad. step^{-1}	b rad.	$\phi_{\mathrm{s}}(x_{\mathrm{s}} = 2$ steps) rad.	$\phi_{\mathrm{s}}(x_{\mathrm{s}} = -2$ steps) rad.
Positive Slit	0.0428	-0.0177	0.068	-0.10
Negative Slit	0.0348	0.00512	0.074	-0.065

cause a condensing lens to focus them at different points associated with the slits. The model produces the Afshar experiment.

8   Discussion

The constants were determined iteratively and with few significant figures. The solution presented may not be unique or optimal.

The $E = mc^2$ relation was used to derive Eq. (3) and (4). This suggests a way to relate measurable quantities to the constants $E = mc^2 = h\nu$. Further, Ψ is responsible for inertial mass. Thus, Ψ is a wave in a "real" physical entity.

The "wave" in quantum mechanics is a wave in the Ψ–field. The hod causes the wave and the wave directs the hod. The speed of the wave in the Ψ–field is much greater than c. Because the number of hods in a *moving* photon determines the wavelength of the Ψ–field wave, the photon causally interacts with other similar hods. Because the wave is a sine or cosine function, matter producing equal wavelength in the Ψ–field can "tune" into each other. This produces the interference pattern. Therefore, quantum entanglement may be a causal and connected observation.

This paper suggests the transverse and longitudinal position of photons undergo forces that may be treated as Fourier transforms with each encounter with more massive particles. The varying Ψ–field experienced by photons causes a Fourier transform on the distribution of photons. Therefore, the probability distribution of the position and movement of the large number of photons may be treated as in quantum mechanics.

The flow of photons through a volume with matter would produce a pattern of waves from each matter particle. Therefore, the Huygen's model of each point being a re-emitter of waves is justified if "each point" means each matter particle such as atoms.

Fourier mathematics assumes an infinite stream of particles obeying a given function for all time. Each encounter with other matter produces a different function. The mathematics of the Fourier transform includes the integration in both time and distance from $-\infty$ to $+\infty$. Therefore, observations made over a region or over a shorter interval allows for the uncertainty of waves. This non-uniformity of the time and distance of the particle stream distribution is Fourier transformed into the Heisenberg Uncertainty Principle (Tang 2007, see, for example, Section 2.9).

The change in the diffraction pattern upon the change in the width of the photon stream that the mask blocks (see Fig. 2) suggests these photons have an influence on the photons that go through the slit. This differs from the traditional wave model of diffraction. It also suggests the photon diffraction experiment is an experiment of quantum entanglement. Indeed, the photons blocked by the mask are non-local to the transmitted photons beyond the mask.

Bell's inequality includes the assumption of locality (Dürr,et al. 2009; Goldstein 2009). Because the present model is intrinsically nonlocal, it avoids Bell's inequality.

The calculation equations allow several negative feedback loops. For example, c is dependent on Ψ. If a photon is at a high Ψ region, c is high. This causes the photon to be faster then the photon producing the wave and move to a lower Ψ. The lower Ψ slows the photon to match the speed of the photon producing the wave. This mechanism exists in θ and v_{t}.

The present concept of "coherent" differs from the traditional model. The photons interact through the Ψ–field and tend toward lower Ψ. Coherence in the sense of interaction of photons is when the photons are maintained at a position and momentum relative to other photons through the feedback mechanisms. This occurs when a photon distribution causes a constant relative, moving minima. That is when $\cos(K_\beta \beta)/r < 1/r$. This also implies there are constant relative forbidden zones where $\cos(K_\beta \beta)/r > 1/r$ and $\Psi \approx \Psi_{\mathrm{max}}$. Thus, position and momentum are quantized.

Knowledge of the density of particles is insufficient to determine the Bohmian quantum potential as noted in Young's experiment. The structure of hods must also be known to provide the Ψ–field. For example, the Ψ–field wave caused by a photon structure of N_{h1} hods differs from the Ψ–field wave caused by a photon structure of N_{h2} hods where $N_{\mathrm{h1}} \neq N_{\mathrm{h2}}$.

Gravity is another manifestation of the Ψ–field–hod interaction. Moving particles produce "pilot waves" (gravity waves) in the Ψ–field. The wave–particle duality of the Copenhagen interpretation may be viewed as which of the two entities (Ψ–field or particle) predominates in an experiment.

For $\theta > \alpha$ the photon's tendency is to align its axis along streamlines of the Ψ–field and axes of other photons. Because of the symmetry of the photon, a converging Ψ–field such as from Sinks and matter and a diverging Ψ–field such as from Sources and galaxy clusters have the same angle changing effect on a photon.

Comparing the SPM and the present model yields the conclusions that the plenum is the Ψ–field and the ρ is the Ψ. A possible addition to the concept of the plenum is that the Ψ–field in the present model supports a transverse wave.

The SPM of the gravitational lens phenomena is that of gravitational attraction changing v_{t} and of $\dot{\theta}$ changing the direction of $\vec{c}$.

Conceptualizing the macroscopic scale of everyday experience, the galactic scale, and the quantum scale can now be done with a single concept as fractal cosmology suggests. The SPM view strengthens the deterministic philosophy. Therefore, the Schrödinger equation represents our lack of knowledge or inability to measure the initial and evolving parameters. The SPM solution for the

Bohmian trajectory(Goldstein 2009) is unique for each particle. The uncertainty of the measurement of position and momentum produces other possible trajectories.

Our measuring instruments measure particles that consist of hods and bound Ψ–field. That is, we measure only particles and their behavior. The properties of the Ψ–field are inferred from how the particles are guided by the Ψ–field and not by measurement of the Ψ–field itself.

Because the plenum is real and because the structure of the photon is consistent with the Michealson-Morley and diffraction experiments, there is no need to introduce action-at-a-distance, length contraction, time dilation, or a single big bang. Because of the unity of concepts between the big and the small, the SPM may be a Theory of Everything.

9   Conclusion

Newton's speculations, Democritus's speculations, the Bohm interpretation, and the fractal philosophy were combined with the cosmological Scalar Potential Model (SPM). The resulting model of photon structure and dynamics was tested by a toy computer experiment.

The simulation of light from a distance produced the diffraction pattern after passing through one and two slit masks. The screen patterns were determined to be diffraction patterns by fitting the pattern on a screen to the Fresnel equation. The distribution that was interpreted as coherent was formed by several lines of photons at angles to $\vec{c}$ consistent with the antenna pattern for the photons with the given N_h. The photons impinging on the opaque portion of the mask were necessary in the calculation. Tracing the path of the photons showed the Fresnel pattern forms after a number of steps from the mask. Also, by varying the distance between the mask and the screen, the Fresnel pattern became the Fraunhofer pattern.

The simulation of Young's experiment showed randomly distributed photons were not coherent but became coherent after passing through one slit. The distribution of photons after the first slit resembled the line pattern of the light from a distance. This pattern was shown to be coherent after passing through a double slit. Young's experiment was duplicated.

The simulation of laser light examined two possible photon distributions. One considered the laser to be emitting pulses of random composition. A Fresnel fit was found. However, the number of minima was inconsistent with the physical structure of the mask. The second posited seed photons formed lines of photons at angles related the N_h. This distribution was also fit by the Fresnel equation and the number of minima was consistent with the mask construction.

Because a model for photon interaction with lenses is lacking, the slit the photon passed through and the position and angle the photons strike the screen were recorded. The average difference of angle depending on the slit the photon passed through could produce the Afshar result. The model is consistent with the Afshar experiment.

Acknowledgments

References

Afshar, S.S., Proceedings of SPIE 5866 (2005): 229-244. preprint http://www.arxiv.org/abs/quant-ph/0701027v1.

Baryshev, Y., Teerikorpi, P., 2004. Discovery of Cosmic Fractals. World Scientific Press.

Bertolami, O., Páramos, J., 2004. Clas. Quantum Gravity 21, 3309.

Descartes, R, 1644. Les Principes de la philosophie. Miller, V. R. and R. P., trans., 1983. Principles of Philosophy. Reidel. http://plato.stanford.edu/entries/descartes-physics/ .

Dürr, D., et al.., 2009. preprint http://arxiv.org/abs/0903.2601.

Eddington, A. S., Space, Time and Gravitation: An Outline of the General Relativity Theory (Cambridge University Press, London, UK).

Goldstein, S., 2009. preprint http://arxiv.org/abs/0907.2427.

Goldstein, S.,Tumulka, R., and Zanghi, N., 2009. preprint http://arxiv.org/abs/0912.2666.

Hodge, J.C., 2004. preprint http://arxiv.org/abs/astro-ph?0409765v1.pdf .

Hodge, J.C., 2006a. NewA 11, 344.

Hodge, J.C., 2006c. preprint http://arxiv.org/abs/astro-ph?0603140v1.pdf .

Hodge, J.C., 2006b. preprint http://arxiv.org/abs/astro-ph?/0611029v2.pdf .

Hodge, J.C., 2006c. preprint http://arxiv.org/abs/astro-ph?0611699v1.pdf .

Hodge, J.C., 2006c. preprint http://arxiv.org/PS_cache/astro-ph/pdf/0612/0612567v2.pdf .

Hodge, J.C., Theory of Everything: Scalar Potential Model of the big and the small(ISBN 9781469987361, available through Amazon.com, 2012).

Lauscher, O. and Reuter, M. 2005. Asymptotic Safety in Quantum Gravity. preprint http://arxiv.org/abs/hep-th?0511260v1.pdf .

Newton, I., Opticks based on the 1730 edition (Dover Publications, Inc., New York, 1952).

Sartori, L., Understanding Relativity(Univ. of California Press, 1996).

Sommerfield, A., 1954. Optics, chaps 5 and 6. Acedemic Press, New York, NY.

Tang, K.T. 1999. Mathematical Methods for Engineers and Scientists 3, Berlin, Germany: Springer–Verlag.

von Flandern, T., 1998. Physics Letters A 250, 1.

Will, C.M., 2001. "The Confrontation between General Relativity and Experiment". Living Rev. Rel. 4: 4-107. http://www.arxiv.org/abs/ gr-qc?0103036.